JOURNAL OF SYNCHROTRON RADIATION
ISSN 1600-5775

A coherent harmonic generation method for producing femtosecond coherent radiation in a laser plasma accelerator based light source

Weihang Liu,[a,b,c] Chao Feng,[d] Yi Jiao[b,c]* and Sheng Wang[a,c]*

[a]China Spallation Neutron Source, Institute of High Energy Physics, Chinese Academy of Sciences, Dongguan, Guangdong 523803, People's Republic of China, [b]Key Laboratory of Particle Acceleration Physics and Technology, Institute of High Energy Physics, Chinese Academy of Sciences, Beijing 100049, People's Republic of China, [c]University of Chinese Academy of Sciences, Beijing 100049, People's Republic of China, and [d]Shanghai Advanced Research Institute, Chinese Academy of Sciences, Shanghai 201210, People's Republic of China.
*Correspondence e-mail: jiaoyi@ihep.ac.cn, wangs@ihep.ac.cn

Received 2 November 2020
Accepted 13 March 2021

Edited by I. Lindau, SLAC/Stanford University, USA

Keywords: laser plasma accelerator-based light source; coherent radiation; transverse–longitudinal coupling; microbunching.

The electron beam generated in laser plasma accelerators (LPAs) has two main initial weaknesses – a large beam divergence (up to a few milliradians) and a few percent level energy spread. They reduce the beam brightness and worsen the coherence of the LPA-based light source. To achieve fully coherent radiation, several methods have been proposed for generating strong microbunching on LPA beams. In these methods, a seed laser is used to induce an angular modulation into the electron beam, and the angular modulation is converted into a strong density modulation through a beamline with nonzero longitudinal position and transverse angle coupling. In this paper, an alternative method to generate microbunching into the LPA beam by using a seed laser that induces an energy modulation and transverse–longitudinal coupling beamlines that convert the energy modulation into strong density modulation is proposed. Compared with the angular modulation methods, the proposed method can use more than one order of magnitude lower seed laser power to achieve similar radiation performance. Simulations show that with the proposed method a coherent pulse of a few microjoules pulse energy and femtosecond duration can be generated with a typical LPA beam.

1. Introduction

Free-electron lasers (FELs) (Madey, 1971) are remarkable tools for scientific experiments. They provide femtosecond-level, extremely intense, and coherent radiation pulses and have opened up huge possibilities for experimental studies in a wide range of scientific fields (Seddon *et al.*, 2017; Rossbach *et al.*, 2019; Fukuzawa & Ueda, 2020). However, these operating FEL facilities, including FLASH (Ackermann *et al.*, 2007), LCLS (Emma *et al.*, 2010), SACLA (Ishikawa *et al.*, 2012), and FERMI (Allaria *et al.*, 2012), are driven by the conventional radiofrequency (RF) linear accelerators. Limited by the breakdown field in metallic materials, the maximal accelerating gradient of the RF technology is below 100 MeV m^{-1} (Dattoli *et al.*, 2017). This limitation, in turn, calls for accelerating structures of hundreds to thousands of meters. These large-scale FEL facilities require a large construction area and cost. Therefore, it is very attractive to reduce the size of the FEL to the university or hospital laboratory scale.

Laser plasma accelerators (LPAs) (Tajima & Dawson, 1979) have emerged as a promising pathway toward this goal. Experiments showed that an LPA can provide a huge accelerating gradient of $\sim$GeV m^{-1} and generate a few GeV

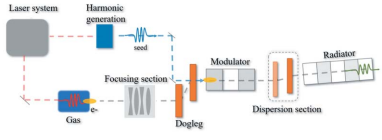

electron beam energy within only a few centimetres distance, with a few percent energy spread, a normalized emittance lower than 1 mm rad, a peak power up to 10 kA, and a beam divergence up to 1 mrad (Esarey *et al.*, 2009; Pollock *et al.*, 2011; Leemans *et al.*, 2014; Thaury, Guillaume, Lifschitz *et al.*, 2015). The LPA-based compact FEL has been widely studied (Huang *et al.*, 2012; Thaury, Guillaume, Dopp *et al.*, 2015; Loulergue *et al.*, 2015; Couprie *et al.*, 2016; Jia & Li, 2017; Qin *et al.*, 2019; Liu *et al.*, 2020). Note that, compared with the electron beam in conventional accelerators, the beam divergence and energy spread of the LPA beam are much larger. Some specific beam manipulations are required to satisfy the light source application requirements. For instance, it has been proposed to use high gradient quadruples or plasma lenses (Thaury, Guillaume, Dopp *et al.*, 2015) to handle the large initial divergence, and chromatic matching (Loulergue *et al.*, 2015; Couprie *et al.*, 2016; Qin *et al.*, 2019) or a transverse gradient undulator (Huang *et al.*, 2012; Zhang *et al.*, 2014; Jia & Li, 2017; Liu *et al.*, 2020) to reduce the effects from the energy spread.

Recently, benefiting from the stable laser system, the stability of the LPA has been greatly improved. For instance, it has been demonstrated (Maier *et al.*, 2020) that energy jitter can be controlled to about 2%. This important milestone brings a positive impetus to LPA applications. Furthermore, spontaneous undulator radiation from LPA beams has been observed experimentally (Schlenvoigt *et al.*, 2008; Fuchs *et al.*, 2009; Anania *et al.*, 2014; André *et al.*, 2018). Stepping further, the forthcoming experiments may focus on coherent undulator radiation (Labat *et al.*, 2020; Alotaibi *et al.*, 2020).

Some coherent harmonic generation (CHG) methods (Feng *et al.*, 2015; Feng *et al.*, 2018; Liu *et al.*, 2019) have been proposed to achieve this goal. These CHG methods use a modulation beamline to generate microbunching structures in the electron bunch. The pre-bunched beam will then radiate coherently in a downstream undulator (called radiator). Note that, because the energy spread of the LPA beam is larger than the gain bandwidth of the FEL, only coherent radiation is generated without further high gain signals.

According to different physical mechanisms, these CHG methods can be classified into two kinds: energy modulation and angular modulation methods. The energy modulation method (Liu *et al.*, 2019) adopts the same modulation beamline as the high-harmonic high-gain (HGHG) scheme used in conventional linac-based FELs (Yu, 1991), which have an undulator (called modulator) and a chicane. The seed laser interacts with the electron beam in the modulator where an energy modulation is generated. Then, in the downstream chicane that offers a longitudinal dispersion, this energy modulation is converted into a density modulation. Generating the nth harmonic of a seed laser typically requires an energy modulation amplitude of n times larger than the initial energy spread. Due to the large energy spread of the LPA beam, the available maximum harmonic number from this method is typically limited to 10, with the corresponding radiation wavelength one order of magnitude longer than that of the soft X-rays (Liu *et al.*, 2019).

On the other hand, the angular modulation methods (Feng *et al.*, 2015; Feng *et al.*, 2018) use the seed laser to modulate the transverse angle (or divergence) of the electron beam. Then a dispersion section providing a coupling between the longitudinal position and transverse angle (instead of longitudinal dispersion) is employed to convert the angular modulation into density modulation. Since the bunching factor of these methods is independent of the initial energy spread and the beam divergence, they can be used to generate high-power EUV or soft X-ray coherent radiation in an LPA-driven light source. To induce an angular modulation, a wavefront-tilted seed laser is adopted by Feng *et al.* (2015); and Feng *et al.* (2018) set the modulator resonant wavelength to the second harmonic of the seed laser (off-resonance condition).

In this paper, we propose an alternative method to generate microbunching structures in the LPA beam by using energy modulation and transverse–longitudinal coupling beamlines. Similar to the angular modulation methods, the bunching factor for the proposed method is independent of the initial energy spread and the beam divergence, promising high-power coherent radiation.

In the proposed method, the seed laser is neither wavefront-tilted nor interacts with an electron beam under off-resonance condition; the required seed laser power is lower than that of the angular modulation methods. In addition, note that the CHG radiation power is proportional to the square of the bunching factor and inversely proportional to the transverse area of the electron beam but nearly independent of the energy spread (Gover, 2005). Unlike the angular methods in which the angular modulation amplitude is controlled to an appropriate level to reach a sufficient bunching factor and avoid an obvious increase in beam divergence and size simultaneously, the proposed method potentially allows using a larger energy modulation amplitude for achieving a larger bunching factor.

Furthermore, as will be shown, by adopting a focusing section (consisting of four quadrupoles) right after the plasma gas, the radiation power of the proposed method can be further improved.

This paper is organized as follows. The details of the proposed method and theoretical derivation of the bunching factor are given in Section 2. In Section 3, we compare the proposed method with the angular modulation methods. In Section 4, numerical examples are presented. In Section 5, the energy jitter effect in the proposed method is investigated. Conclusions are given in Section 6.

2. Method

We consider a TW-level laser system that simultaneously delivers two pulses (or one pulse splits into two pulses). The main laser pulse is focused in a gas medium for trapping and acceleration of the electron beam. The second laser pulse is used for seed generation (see Fig. 1). With this setting, the time synchronization between the seed laser and the electron beam may be achieved easily.

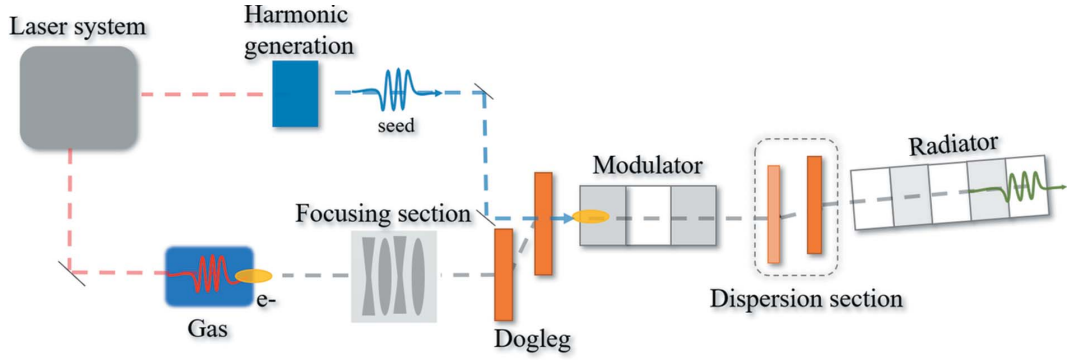

Figure 1
Schematic of the proposed method for microbunching generation and coherent radiation.

The modulation beamline contains a focusing section, a dogleg, a modulator, and a dispersion section. Note that the focusing section is optional and does not affect the microbunching generation. We will derive the bunching factor without considering the focusing section, and revisit it at the end of this section. To analyze the modulation process and find the optimal condition of the bunching factor, we adopt the beam transport matrix to track the 4D phase-space evolution of the electron in the modulation beamline. The 4D phase space coordinates of the electron are defined by (x, x', z, δ), where x is the transverse position, x' is the transverse angle, z is the longitudinal position, and δ is the energy deviation.

The 4×4 transport matrix for the dogleg is (Chao *et al.*, 2013)

$$M_{\rm d} = \begin{bmatrix} 1 & L_{\rm d} & 0 & \eta_{\rm d} \\ 0 & 1 & 0 & 0 \\ 0 & \eta_{\rm d} & 1 & \zeta_{\rm d} \\ 0 & 0 & 0 & 1 \end{bmatrix}, \tag{1}$$

where $L_{\rm d}$, $\eta_{\rm d}$ and $\zeta_{\rm d}$ are the length, transverse dispersion and longitudinal dispersion of the dogleg, respectively.

The dispersion section consists of two dipoles separated by a drift and having different bending angles. The transport matrix for the dispersion section can be written as

$$M_{\rm ds} = \begin{bmatrix} 1 & L_{\rm ds} & 0 & \eta_{\rm ds} - \theta_{\rm ds} L_{\rm ds} \\ 0 & 1 & 0 & -\theta_{\rm ds} \\ \theta_{\rm ds} & \eta_{\rm ds} & 1 & \zeta_{\rm ds} \\ 0 & 0 & 0 & 1 \end{bmatrix}, \tag{2}$$

where $L_{\rm ds}$, $\theta_{\rm ds}$, $\eta_{\rm ds}$ and $\zeta_{\rm ds}$ are the length, z–x coupling term, z–x' coupling term and longitudinal dispersion of the dispersion section, respectively.

The energy modulation process in the modulator with length $L_{\rm m}$ can be modeled as a transport matrix $M_{\rm m}$ and an energy kick $\Delta\delta$ at the modulator center. The transport matrix $M_{\rm m}$ of a linearly polarized undulator is (Balandin & Golubeva, 2017)

$$M_{\rm m} = \begin{bmatrix} 1 & L_{\rm m} & 0 & 0 \\ 0 & 1 & 0 & 0 \\ 0 & 0 & 1 & 2\zeta_{\rm m} \\ 0 & 0 & 0 & 1 \end{bmatrix}, \tag{3}$$

where $\zeta_{\rm m}$ is the half longitudinal dispersion of the modulator.

The energy kick $\Delta\delta$ is

$$\Delta\delta = A_{\rm m}\sigma_\delta \sin(k_{\rm L} z), \tag{4}$$

where $A_{\rm m}$ is the amplitude of the energy modulation in the unit of initial energy spread σ_δ, and $k_{\rm L}$ is the wavenumber of the laser. For a given $A_{\rm m}$, the required seed laser power is

$$P = \frac{P_0 z_{\rm r}}{2k_{\rm L}} \frac{A_{\rm m}^2 \gamma^4}{[JJ]^2 K^2 L_{\rm m}^2} (\sigma_\delta)^2, \tag{5}$$

where K is the undulator parameter, $P_0 = mc^3/r_{\rm e}$, $r_{\rm e}$ is the classical electron radius, $z_{\rm r}$ is the Rayleigh length, $[JJ] = J_0(\xi) - J_1(\xi)$, with $\xi = K^2/(2 + K^2)$.

After passing the modulation beamline, the longitudinal coordinate of an electron with initial coordinates $(x_0, x_0', z_0, \delta_0)$ changes to

$$\begin{aligned} z_{\rm f} = {} & z_0 + A_1 x_0 + A_2 x_0' + A_3 \delta_0 \\ & + r_{56} A_{\rm m} \sigma_\delta \sin\left[k_{\rm L}(\eta_{\rm d} x_0' + z_0 + \zeta_{\rm d}\delta_0 + \zeta_{\rm m}\delta_0)\right], \end{aligned} \tag{6}$$

in which

$$\begin{aligned} r_{56} &= \zeta_{\rm ds} + \zeta_{\rm m}\,, \\ A_1 &= \theta_{\rm ds}\,, \\ A_2 &= \eta_{\rm ds} + \eta_{\rm d} + (L_{\rm m} + L_{\rm d})\,\theta_{\rm ds}\,, \\ A_3 &= r_{56} + \zeta_{\rm m} + \zeta_{\rm d} + \eta_{\rm d}\theta_{\rm ds}. \end{aligned} \tag{7}$$

Based on the definition of the bunching factor at the nth harmonic (Kim *et al.*, 2017),

$$b_n = \left| \int \exp(-in k_{\rm L} z_{\rm F}) f(x_0, x_0', z_0, \delta_0)\, {\rm d}x_0\, {\rm d}x_0'\, {\rm d}z_0\, {\rm d}\delta_0 \right|, \tag{8}$$

and assuming the initial distribution $f(x_0, x_0', z_0, \delta_0)$ to be Gaussian, we find

$$\begin{aligned} b_n = {} & \left| \sum_{j=-\infty}^{\infty} J_j(n k_{\rm L} r_{56} \sigma_\delta A_{\rm m}) \right. \\ & \times \exp\left(\frac{-(k_{\rm L})^2}{2} \left\{ (nC_1\sigma_{x_0})^2 + \left[nC_2 + (n-j)\eta\right]^2 \sigma_{x_0'}^2 \right. \right. \\ & \left. \left. + \left[nC_3 + (n-j)\zeta_{\rm d}\right]^2 \sigma_\delta^2 + (n-j)^2 \sigma_{z0}^2 \right\} \right) \Bigg|, \end{aligned} \tag{9}$$

with

$$C_1 = \theta_{ds},$$
$$C_2 = \eta_{ds} + (L_m + L_d)\,\theta_{ds}, \quad (10)$$
$$C_3 = r_{56} + \eta_d \theta_{ds},$$

where σ_{x0}, $\sigma_{x_0'}$ and σ_{z0} are the initial beam size, initial beam divergence and initial bunch length, respectively.

Under the condition $k_L\sigma_z \gg 1$, the bunching factor [equation (9)] is reduced to

$$b_n = \left|J_n(nk_L r_{56}\sigma_\delta A_m)\right| \times \exp\left[\frac{-(k_L n)^2}{2}\left(C_1^2\sigma_{x_0}^2 + C_2^2\sigma_{x_0'}^2 + C_3^2\sigma_\delta^2\right)\right]. \quad (11)$$

To minimize the influence of the initial large beam divergence and energy spread, we take $C_2 = 0$ and $C_3 = 0$.

Under these conditions, by introducing the parameters A and B,

$$A = A_m \frac{\sigma_\delta \eta_d}{\sigma_{x_0}}, \quad (12)$$

$$B = k_L r_{56} \frac{\sigma_{x_0}}{\eta_d}, \quad (13)$$

the bunching factor can be expressed in the following compact form,

$$b_n = \left|J_n(nAB)\right| \exp\left[\frac{-(nB)^2}{2}\right]. \quad (14)$$

This form does not only apply to the energy modulation method but also to angular modulation methods (Yu, 1991; Xiang & Wan, 2010). In the next section, we will compare the proposed method with the angular modulation methods proposed by Feng *et al.* (2015) and Feng *et al.* (2018), based on this formula.

According to the property of the Bessel function, the nth-order ($n > 4$) Bessel function reaches the first maximum ($\sim 0.67n^{-1/3}$) when its argument is equal to $n + 0.81n^{1/3}$. So to maximize the bunching factor, the J_n factor in equation (14) should be maximized by choosing

$$AB = 1 + 0.81n^{-2/3}. \quad (15)$$

And the exponential factor should be close to 1, which suggests $B \leq n^{-1}$. Combining equation (15), we have $A \geq n$.

Different values of A will result in different optimal bunching factors. In the case of the smallest A, *i.e.* $A = n$, the optimal bunching factor is around $0.41n^{-1/3}$. In the case of large A for instance, $A = 4n$, the optimal bunching factor is around $0.65n^{-1/3}$. Note that when $A > 4n$, compared with $A = 4n$, the maximum increase of the optimal bunching factor is only about 3%. So $4n$ is sufficient to obtain a larger bunching factor. From equation (12), this requires a sufficiently larger energy modulation amplitude A_m or a larger dispersion η_d.

Before the dogleg, one can adopt a focusing section to control the beam envelope and to optimize the radiation power. The focusing section has no coupling between the longitudinal and transverse dimensions, hence it has no effect on the generation of microbunching. In this case, the beam size σ_{x_0} needs to be replaced by $(\varepsilon_x\beta_x)^{1/2}$, where ε_x is the horizontal emittance, and β_x is the horizontal beta function at the entrance of the dogleg.

3. Comparison with the angular modulation methods

To compare the proposed method with the angular modulation methods, we will first review the wavefront-tilted laser method (Feng *et al.*, 2015) and the off-resonance modulation method (Feng *et al.*, 2018) in Sections 3.1 and 3.2, and make numerical comparison among these methods in Section 3.3.

3.1. Wavefront-tilted laser method

In this method, the seed laser interacts with the electron beam in the modulator with a tilt angle τ (the angle between the direction of the electron propagation and the direction of the incident seed laser). With this setting, the magnetic field of the seed laser will have a longitudinal component. This field interacts with the transverse wiggling electron, which generates an angular modulation into the electron beam.

For this method, the parameter A can be written as

$$A = A_a \frac{\sigma_{x_0'} L_{drift}}{\sigma_{x_0}}, \quad (16)$$

where A_a is the the amplitude of the angular modulation in the unit of initial beam divergence $\sigma_{x_0'}$ and L_{drift} is the drift length between the electron source and the modulator.

Note that this method also induces an energy modulation. The energy modulation amplitude A_m and the angular modulation amplitude A_a are related by

$$A_m = A_a \frac{\sigma_{x_0'}}{\sigma_\delta \tau}. \quad (17)$$

This energy modulation is useless and will increase the energy spread. Under given A_a and beam parameters, a larger τ is preferred to induce a smaller A_m and a weaker energy disturbance to the electron beam.

The laser tilted angle τ is related to the laser wavelength λ_L and the modulator period λ_u through the resonance condition (Wang *et al.*, 2019)

$$\lambda_L = \frac{\lambda_u}{2\gamma^2}\left(1 + \frac{K^2}{2} + \gamma^2\tau^2\right). \quad (18)$$

The seed laser power required for obtaining A_a is

$$P = \frac{P_0 z_r}{2k_L} \frac{A_a^2\gamma^4}{[JJ]^2 K^2 L_m^2} \left(\frac{\sigma_{x_0'}}{\tau}\right)^2. \quad (19)$$

Combining equations (18) and (19) we find that, for given λ_u, when

$$\tau \simeq \left(\frac{\lambda_L}{\lambda_u} - \frac{1}{2\gamma^2}\right)^{1/2}, \quad (20)$$

the seed laser power is minimized. As mentioned, to reduce the disturbance to the beam energy, a large τ is preferred, which corresponds to a short modulator period.

In addition, since in the modulator the center of the tilted laser gradually deviates from the electron beam center, the long modulator may induce inhomogeneous modulation in the transverse plane. To mitigate this effect, a different modulator length may require a different laser waist size. For short and long modulators, the laser waist size should be proportional to $L_{\rm drift}\,\sigma_{x_0'}$ and $\tau L_{\rm m}$, respectively. The ratio between the seed laser power of the short and the long modulator is

$$\frac{P_{\rm S}}{P_{\rm L}} = \left(\frac{L_{\rm drift}\,\sigma_{x_0'}}{N\lambda_{\rm u}}\right)^2, \tag{21}$$

where N is the period number of the short modulator. For typical values with $L_{\rm drift} \simeq 1$ m, $\sigma_{x_0'} \simeq 0.1$ mrad, $\lambda_{\rm u} \simeq 1$ cm and $N = 2$, $P_{\rm S}$ is about four orders of magnitude smaller than $P_{\rm L}$. Therefore, it is more attractive to use a short modulator.

3.2. Off-resonance modulation method

In this method, the modulator resonates at the second harmonic of the seed laser. When the electron beam passes one period of the modulator, the seed laser slips ahead by half a wavelength, which will result in a nonzero angular modulation into the electron beam.

The parameter A and the angular modulation amplitude $A_{\rm a}$ satisfy the same relationship as those of the wavefront-tilted laser method [equation (16)].

The energy modulation amplitude $A_{\rm m}$ of this method can be written as

$$A_{\rm m} = A_{\rm a}\left(\frac{2\lambda_{\rm u}}{\lambda_{\rm L}}\right)^{1/2}\frac{\sigma_{x_0'}}{\sigma_\delta}. \tag{22}$$

Again, to induce a weak energy disturbance, a short modulator period is preferred.

The seed laser power required for a given $A_{\rm a}$ is

$$P = \frac{P_0 k_{\rm L} z_{\rm r}}{2\pi^2}\frac{A_{\rm a}^2\gamma^2}{[gg]^2}\left(\sigma_{x_0'}\right)^2, \tag{23}$$

with

$$[gg] = g_{1/4}\left(\frac{\xi}{4}\right) - \frac{\xi}{2}g_{-3/4}\left(\frac{\xi}{4}\right) - \frac{\xi}{2}g_{5/4}\left(\frac{\xi}{4}\right),$$

$$g_\nu(\chi) = \frac{1}{\pi}\int_0^\pi \left[\cos(\chi\sin t - \nu t) + \sin(\chi\sin t - \nu t)\right]{\rm d}t.$$

Note that $[gg]$ is determined by the modulator parameter K. When K is larger than 1, $[gg]$ is around 1.3. In the modulator, K is typically larger than 1, so for fixed $A_{\rm a}$, $\lambda_{\rm L}$, $z_{\rm r}$ and beam parameters, the seed laser power is independent of $\lambda_{\rm u}$.

3.3. Numerical comparison

Here, we use the beam parameters listed in Table 1 and assume that the period number of the modulator is 2, the Rayleigh length is 2.78 m and the harmonic number n is 20. For angular modulation methods, the drift length is selected as 3 m. To obtain the same modulation amplitudes in the proposed method and the angular modulation methods, from equations (12) and (16), the dispersion of the dogleg $\eta_{\rm d}$ in the proposed method is set to 0.75 cm.

Table 1
Parameters for the LPA beam.

Beam parameter	Value	Unit
Beam energy	1	GeV
Energy spread (RMS)	1%	
Normalized emittance	0.1	μm
Beam size (RMS)	2	μm
Bunch length (RMS)	1	μm
Peak current	10	kA

Table 2
Case for small modulation amplitude (b_{20} = 15%).

Method	Proposed	Wavefront-tilted	Off-resonance modulation
Seed power (TW)	0.075	0.95	13.5
$\lambda_{\rm u}$ (cm)	40	4	6
K	2.82	7.05	5.58
Laser tilt angle (mrad)	0	2.50	0
Induced divergence (μrad)	0	9.37	9.37
Induced energy spread	0.375%	0.375%	0.77%

Table 3
Case for large modulation amplitude (b_{20} = 24%).

Method	Proposed	Wavefront-tilted	Off-resonance modulation
Seed power (TW)	1.17	14.56	208.65
$\lambda_{\rm u}$ (cm)	40	4	6
K	2.82	7.05	5.58
Laser tilt angle (mrad)	0	2.50	0
Induced divergence (μrad)	0	37.26	37.26
Induced energy spread	1.49%	1.49%	3.06%

As has been mentioned in Section 2, parameter A should be larger or equal to n. And there are mainly two kinds of options for A (*i.e.* $A = n$ and $A = 4n$). In the following, we consider these two options separately and list the corresponding main parameters in Tables 2 and 3.

For $A = n = 20$, the optimal bunching factor is about 15%. The modulation amplitudes for the proposed method ($A_{\rm m}$) and the angular modulation methods ($A_{\rm a}$) are all equal to 0.53 (*i.e.* $A_{\rm m} = A_{\rm a} = 0.53$). The seed laser powers as a function of $\lambda_{\rm u}$ are shown in Fig. 2. For the wavefront-tilted laser method, the seed laser power for different $\lambda_{\rm u}$ is calculated at the value of τ from equation (20). To control the seed laser power, a small $\lambda_{\rm u}$ is required. Here we choose $\lambda_{\rm u}$ as 4 cm. The corresponding seed laser power and the seed laser tilted angle τ is 0.95 TW and 2.5 mrad, respectively. Note that a smaller $\lambda_{\rm u}$ can only slightly reduce the seed laser power. For example, when $\lambda_{\rm u}$ is 3 cm, the seed laser power is reduced only by about 2%, but the corresponding peak magnetic field, $B_0 = 2\pi mcK/(e\lambda_{\rm u})$, of the modulator is larger than 2.8 T, which will bring great technical challenges. For the off-resonance modulation method, the seed laser power is about 13.5 TW for all $\lambda_{\rm u}$. Here, we choose a $\lambda_{\rm u}$ of 6 cm under the consideration of inducing a small energy disturbance and technical limitations of the

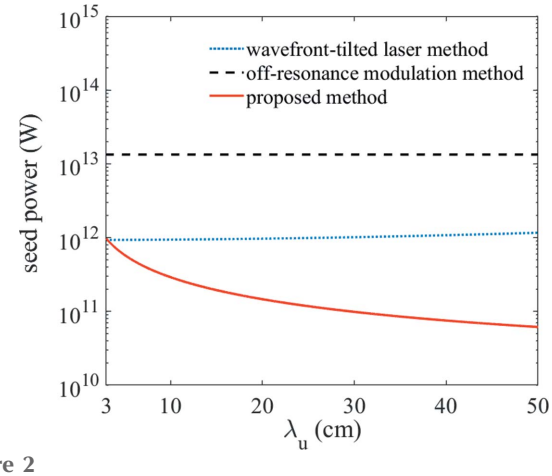

Figure 2
The required laser power as a function of modulator period λ_u for three different methods.

undulator. For the proposed method, the seed laser power decreases with λ_u. One can choose such a large λ_u that the seed laser power is more than one order of magnitude smaller than that of the angular modulation methods. For example, when $\lambda_u = 40$ cm, the seed laser power of the proposed method is only about 0.075 TW.

For $A = 4n = 80$, the optimal bunching factor is about 24%. The modulation amplitude for the three methods is 2.1. In this case, the seed laser of the angular modulation methods exceeds 10 TW, which will cause a large increase in beam divergence (about $1.49\,\sigma_{x_0'}$). In contrast, the proposed method requires only a seed laser of 1.17 TW and does not cause an additional increase of the beam divergence. Note that, when the electron beam passes through the radiator, a large increase in beam divergence will lead to a rapid increase in beam size and a decrease in radiation power; the proposed method seems more suitable for taking a larger A to increase the bunching factor for a higher CHG output power.

On the other hand, as will be shown in Section 5, due to the dispersion induced by the dogleg, the tolerance of the radiation power to the energy jitter of the proposed method is more stringent compared with the angular modulation methods. Nevertheless, once the energy jitter of the LPA beam is controlled to be sufficiently small, *e.g.* below 2%, the proposed method requiring lower seed laser power appears more favorable than these two angular modulation methods.

4. Application in LPA

To verify the feasibility of the proposed method, we consider generating coherent radiation with a wavelength of the 20th harmonic of a 260 nm seed laser. We track the electrons in the beamline with *ELEGANT* (Borland, 2001), taking into account the third-order transport effect and the coherent synchrotron radiation (CSR) effect. The interaction between electrons and seed laser in the modulator and the radiation processes in the radiator are simulated with *Genesis* (Reiche, 1999). The electron beam parameters used in the simulation are shown in Table 1. And the initial distribution is assumed to be Gaussian.

In the dogleg design, two effects should be considered. The first is bunch lengthening, which can be expressed as

$$\sigma_z = \left[\sigma_{z_0}^2 + \left(\eta_d \sigma_{x_0'}\right)^2 + \left(\zeta_d \sigma_\delta\right)^2\right]^{1/2}. \tag{24}$$

This effect will reduce the peak current and decrease the radiation power. Another effect is the CSR effect, which will lead to energy spread and emittance increases (Brynes *et al.*, 2018). To mitigate these effects, two dipoles with small bending angles are needed to construct a compact dogleg.

To achieve a large bunching factor, parameter A is chosen to be around $4n = 80$. Considering the small bending angle requirement of the dogleg, we choose a sufficiently large energy modulation amplitude A_m while maintaining the dispersion η_d to a small level. Typically, A_m should be smaller than 10 for a weak energy disturbance. Here we select A_m to be 3. The corresponding increase in energy spread is about $2\sigma_\delta$. From equation (12), the dispersion η_d is about 0.5 cm, with the corresponding bending angle of 20 mrad.

Under those parameters, the peak current is decreased by about 17.4% (from 10 to ~8.26 kA) after passing through the dogleg, as shown in Fig. 3.

From equations (13) and (15), the optimal r_{56} is 1.53 µm. Combining $C_2 = 0$ and $C_3 = 0$, we find $\theta_{ds} = -0.3$ mrad and $\eta_{ds} = 0.4$ mm. Taking half of the modulator into account, the

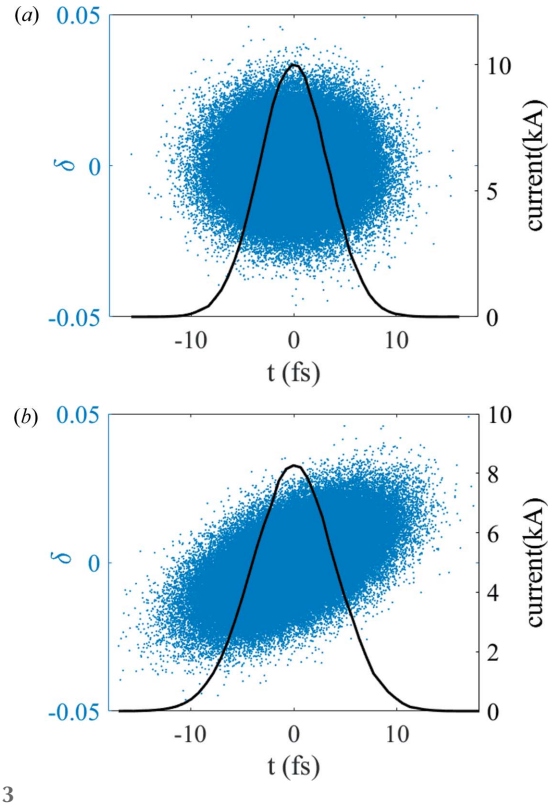

Figure 3
Longitudinal phase space distributions (blue dots) and current profiles (black curves) before (*a*) and after (*b*) the dogleg. The bunch head is on the right.

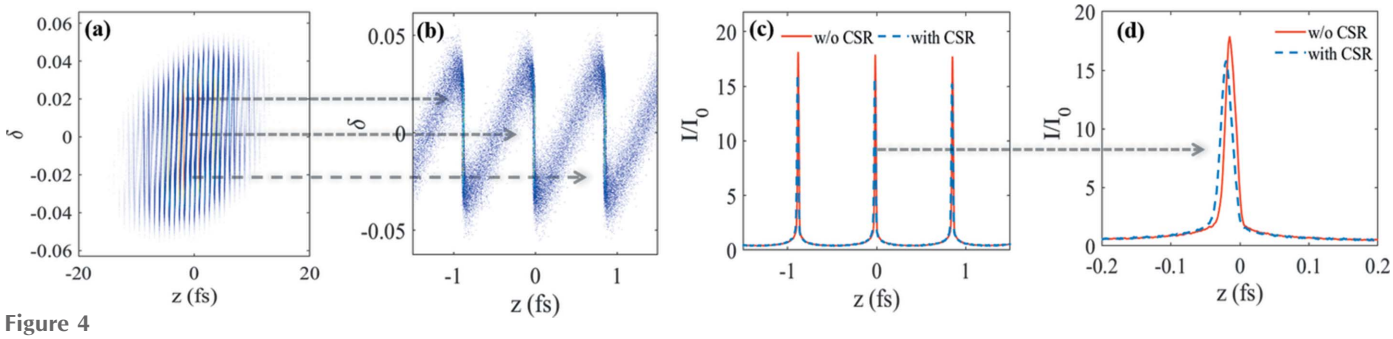

Figure 4
Panel (*a*) shows the longitudinal phase space of the beam at the entrance of the radiator. The enlarged phase space from (*a*) is given in (*b*). Panel (*c*) shows the corresponding current profiles for the cases with (blue dash curve) and without (red curve) considering the CSR effect. The enlarged current profiles from (*c*) are given in (*d*).

Table 4
Parameters for the seed laser, modulation beamline and the radiator.

	Value	Unit
Seed laser		
Rayleigh length	2.78	m
Peak power	2	TW
Rms duration	20	fs
Dogleg		
Bending angle	20	mrad
Bend length	0.25	m
Dispersion section (optimal bunching factor @ entrance of radiator)		
Bending angle for first dipole	−3.4	mrad
Drift	0.06	m
Bending angle for second dipole	3.1	mrad
Bend length	0.08	m
Dispersion section (optimal bunching factor @ 19th period of radiator)		
Bending angle for first dipole	−1.63	mrad
Drift	0.23	m
Bending angle for second dipole	1.31	mrad
Bend length	0.1	m
Radiator		
Period	3	cm
Period number	24	

longitudinal dispersion $\zeta_{\rm ds}$ is about 1.17 µm. The detailed parameters of the dogleg and dispersion section are listed in Table 4.

After passing through the dispersion section, micro-bunching structures are generated in the electron beam (see Fig. 4). The bunching factors for different harmonic numbers are calculated and shown in Fig. 5. From Fig. 5, one can see that the bunching factor is degraded when the CSR effect is considered. Previous studies (Deng *et al.*, 2011; Hemsing, 2018) have shown that this degradation is due to the CSR-induced energy modulation. For the target harmonic number at 20, the bunching factor is about 19.5%. Even at the 50th harmonic (corresponding to the wavelength of 5.2 nm), the bunching factor is around 3%, which is still larger than the shot noise, suggesting that the modulated electron beam with the proposed method can radiate coherently at the soft X-ray regime.

By injecting the pre-bunched electron beam into the radiator, as can be seen in Fig. 6, the bunching factor oscillates

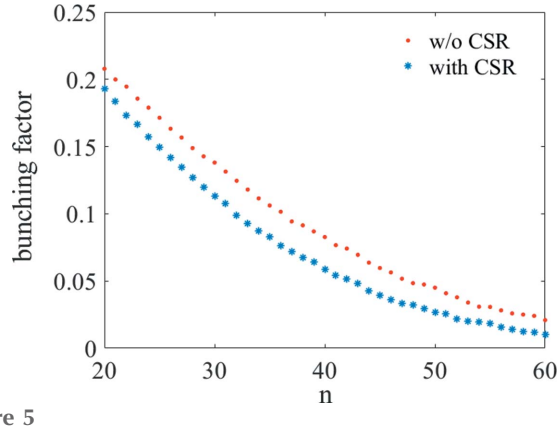

Figure 5
The bunching factor as a function of different harmonic numbers for the cases with (blue star points) and without (red dot points) considering the CSR effect.

with a large damping ratio (the first maximum is five times larger than the second maximum) leading to premature saturation of the radiation power. The maximum radiation power is obtained at position ∼0.3 m with a value of about 60 MW. To improve the radiation power, we take the contribution of the longitudinal dispersion of an N (N is smaller than the total periods of the radiator) periods radiator $\zeta_{N\text{-rad}}$ into the optimal r_{56},

$$r_{56} = \zeta_{\rm m} + \zeta_{\rm ds} + \zeta_{N\text{-rad}}. \quad (25)$$

In this way, the optimal bunching factor will be obtained after N periods of the radiator to bring about the continuous increase of the radiation power, and avoid premature saturation and improve the radiation output. After a simple scan, it is found that N = 19 results in a maximum radiation power. In this case, the maximum bunching factor is about 16.7% [see Fig. 6(*a*)]. Although this value is about 14% lower than the previous one (∼19.5%), the continuous increase of the bunching factor causes the radiation power to saturate at the end of the radiator, and the maximum power is six times larger, ∼368 MW [see Fig. 6(*b*)]. The FEL pulse transverse profiles for the cases with optimal bunching factor at z = 0 m and at z = 0.57 m are shown in the insert of Fig. 6(*b*). In these two cases, similar profile shapes and the same spot sizes (about 0.13 mm) are obtained. However, the degrees of the trans-

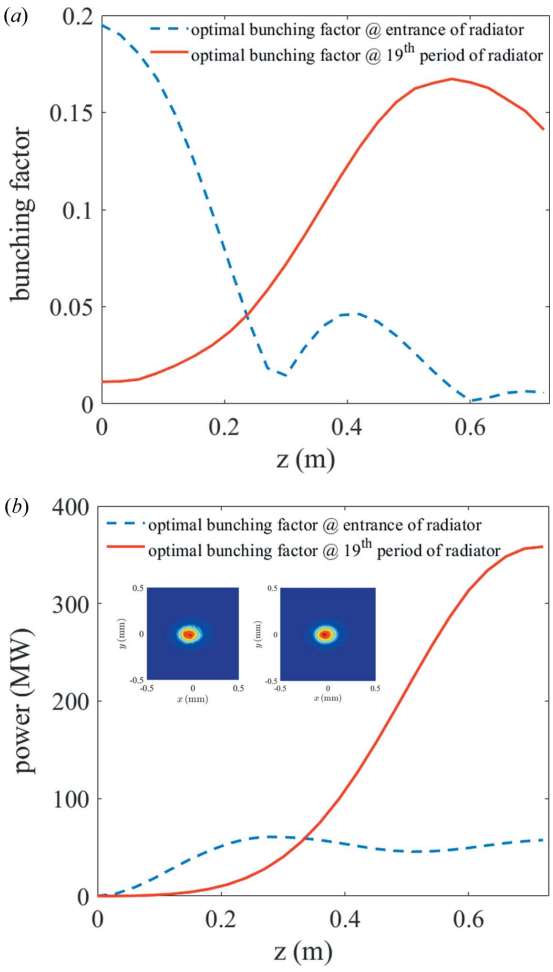

Figure 6
The bunching factor (*a*) and radiation power (*b*) as a function of z for the cases with optimal bunching factor at z = 0 m (dashed blue) and with optimal bunching factor at z = 0.57 m (solid red). The insert plots are the FEL pulse transverse profiles for the cases with optimal bunching factor at z = 0 m (left) and with optimal bunching factor at z = 0.57 m (right).

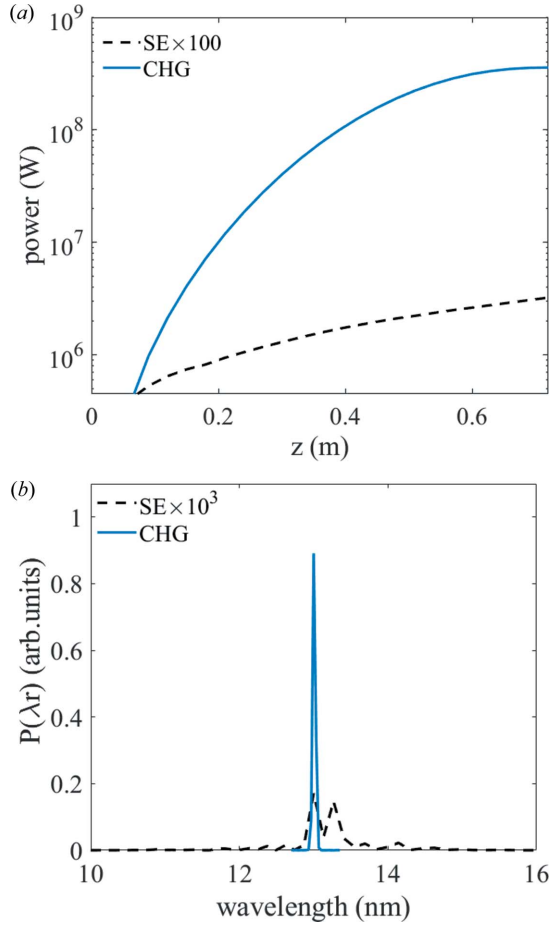

Figure 7
(*a*) Peak power gain curves for the CHG (solid blue) and SE (dashed black). (*b*) Spectra for the CHG (solid blue) and SE (dashed black).

verse coherence (D_{tr}) of these two cases are different. For the case with optimal bunching factor at z = 0 m, D_{tr} is about 62%, while for the case with optimal bunching factor at z = 0.57 m, D_{tr} is about 93%.

We also compare the output radiation from the proposed method with that of the spontaneous emission (SE) by directly sending the LPA beam into the radiator. As can be seen from Fig. 7, the output radiation power with the proposed method is more than three orders of magnitude higher than the SE power. And, the RMS bandwidth of the CHG spectrum is about 0.16%, that is over one order of magnitude narrower than that of the SE. The RMS time duration of the CHG radiation pulse is about 2.53 fs, and the time-bandwidth product of this coherent pulse is 0.59, which is close to the Fourier transform-limited value (0.5).

To further improve the radiation performance of the proposed method, we adopt a four-quadrupole focusing section close to the beam source point to control the beam size evolution in the modulation beamline. Due to the large beam divergence at the beam source point, strong quadrupoles are needed to focus the beam; while, on the other hand, the strong focusing and large beam energy spread induce large chromatic effects that will increase the emittance. One way to mitigate this emittance growth is to adopt sextupoles in the nonzero dispersion position. Here, to design a compact and simple beamline, we adopt the apochromatic design (Lindstrøm & Adli, 2016). In this design, the first or even high-order derivative of the Twiss function versus δ is minimized by carefully adjusting the strength and position of the quadrupoles. The maximum gradient of these quadrupoles is about 250 T m^{-1}. The gradient is high but achievable with permanent-magnet technology (Ghaith *et al.*, 2018, 2019).

As shown in Figs. 8(*a*) and 8(*b*), at the entrance of the dogleg, for different energy deviations (from −6% to 6%) the maximum variation of the beta and alpha functions is below 43% and 3%, respectively. In the modulator and radiator, the average beam sizes are controlled to be below 52 µm and 65 µm, respectively [see Fig. 8(*c*)]. Benefiting from this, the maximum bunching factor in the radiator is increased by about 12% [see Fig. 9(*a*)], and the output radiation power is five times larger than the case without the focusing section.

Another advantage of using the focusing section is that the tolerance of the radiation power to beam divergence can be improved. As shown in Fig. 10, when the beam divergence

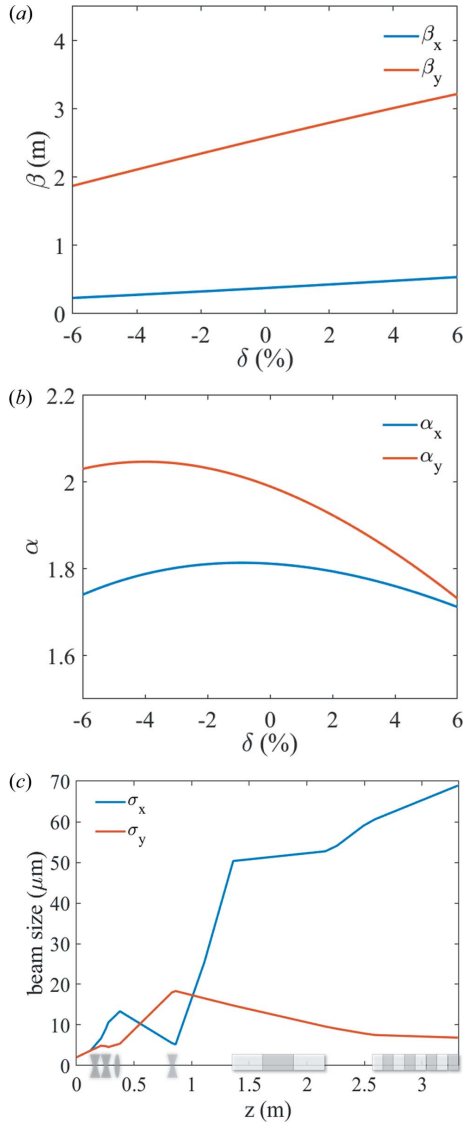

Figure 8
Plots (*a*) and (*b*) show the Twiss functions varied with energy deviation at the entrance of the dogleg. Plot (*c*) shows the beam sizes varied along z for the case with the focusing section.

increases from 25 to 150 μrad, the radiation power reduction is about one order of magnitude; while for the case without the focusing section, this reduction is close to two orders of magnitude.

5. Energy jitter investigation

An energy jitter will cause resonance wavelength detuning. Additionally, the beam energy jitter δ_c, together with the dispersion of the dogleg, will drive a time delay $\Delta t = -\xi_d \delta_c / c$ and a transverse position offset $\Delta x = \eta_d \delta_c$. These energy jitter induced effects will reduce the energy modulation amplitude A_m, and hence decrease the bunching factor of the proposed method. Note that, for the angular modulation methods, energy jitter will only induce the wavelength detuning.

To investigate the impact of these effects, we calculate the energy modulation amplitude and the bunching factor (at the

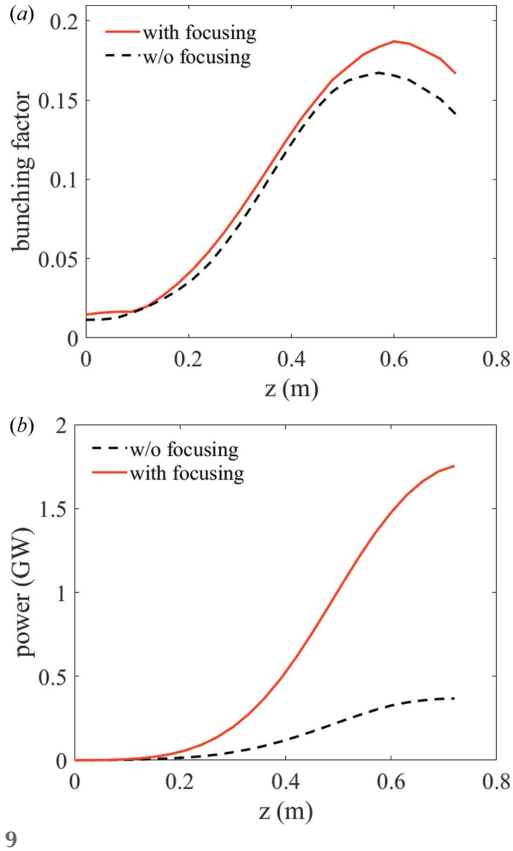

Figure 9
(*a*) Bunching factor at the 20th harmonic varied along the radiator for the cases with (solid red) and without the focusing section (dashed black). (*b*) Peak power gain curves for the cases with (solid red) and without the focusing section (dashed black).

harmonic number 20) for different values of energy jitter. The results are shown in Fig. 11. For the proposed method, to obtain a bunching factor that is usually one or two orders of magnitude larger than the shot noise (about 10^{-5}), the energy jitter should be smaller than 5% [see the red cross in Fig. 11(*b*)]. If only the wavelength detuning effect is considered (which can be regarded as the case of using the angular modulation methods), the energy jitter will only need to be

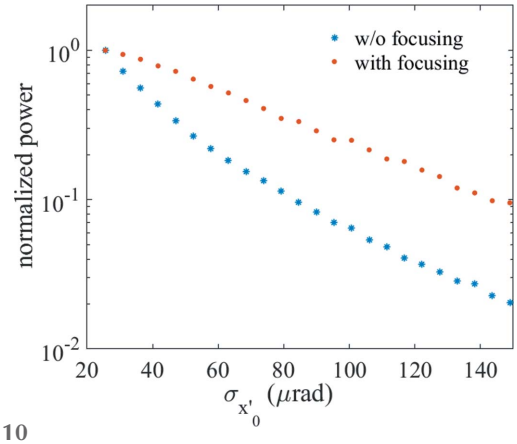

Figure 10
Normalized power as a function of initial beam divergences for the cases without (blue star points) and with (red dot points) the focusing section.

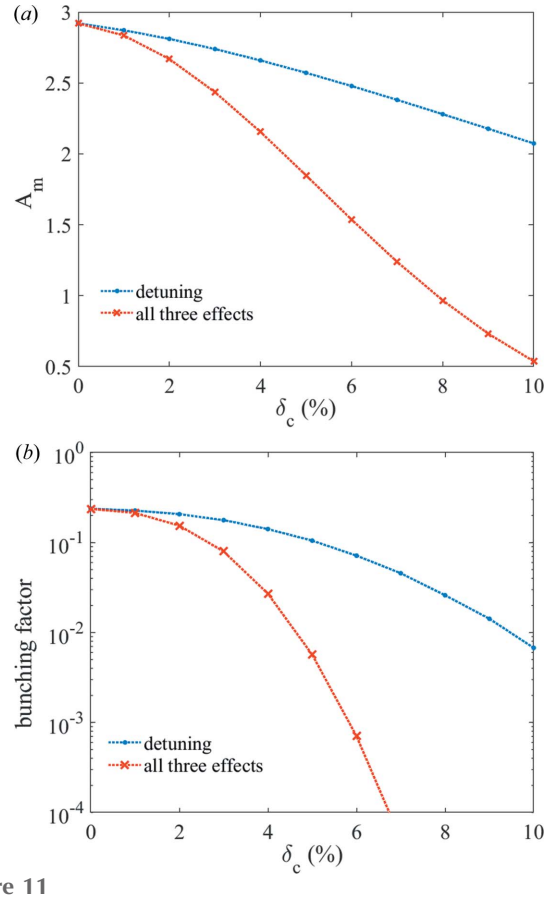

Figure 11
The energy modulation amplitude (*a*) and bunching factor (*b*) as a function of the energy jitter for different effects: detuning (blue dots) and the combination of detuning, time delay and transverse position offset effects (red cross).

smaller than 10% to meet the same requirement for the bunching factor.

Luckily, the recent experiment shows that the energy jitter can be controlled to around 2% with a stable laser system (Maier *et al.*, 2020). At this energy jitter level, the difference between the bunching factor of the angular modulation methods and the proposed method is less than 4%.

Note that the time delay and the transverse position offset effects can be mitigated by using a seed laser with a longer pulse duration and larger transverse size, of course, with a price of higher seed laser energy.

6. Conclusions

A compact modulation beamline to generate a fully coherent femtosecond radiation pulse with EUV or soft X-ray wavelength for an LPA-based light source has been proposed. This beamline consists of a dogleg, a dispersion section, and two short undulators. The dogleg and the dispersion section induce transverse–longitudinal couplings, which enables a bunching factor independent of the beam divergence and energy spread. Benefiting from this, a large bunching factor can be obtained at high harmonics. Simulations show that the proposed method can be used to generate a coherent pulse with microjoule level pulse energy and femtosecond duration.

Compared with the angular modulation methods given by Feng *et al.* (2015) and Feng *et al.* (2018), the proposed method can obtain the same bunching factor with lower laser power. And since the proposed method is based on energy modulation, a larger modulation amplitude can be used to obtain a larger bunching factor for even higher radiation power. Nevertheless, the proposed method has a smaller energy jitter tolerance. Thus, a more stable laser system for LPA is essentially important to achieve a small energy jitter.

The investigation of the CSR effect shows that CSR has a nonignorable impact on the bunching factor. Nevertheless, it is possible to mitigate this effect, for example, using the method shown by Khan & Raubenheimer (2014).

It is worth noting that this method is not limited to the application in LPA-based light sources, but can also be applied in conventional linac-based FELs or storage-ring-based light sources.

Acknowledgements

We thank Senlin Huang (Peking University) and Dao Xiang (Shanghai Jiao Tong University) for useful comments. We acknowledge Gang Zhao (Peking University) and Sheng Zhao (Peking University) for the fruitful discussions on numerical simulation.

Funding information

The following funding is acknowledged: National Key Research and Development Program of China (grant No. 2016YFA0401900); Youth Innovation Promotion Association of the Chinese Academy of Sciences (grant No. Y201904); Bureau of Frontier Sciences and Education, Chinese Academy of Sciences (grant No. QYZDJ-SSW-SLH001); National Natural Science Foundation of China (grant No. 11922512).

References

Ackermann, W., Asova, G., Ayvazyan, V., Azima, A., Baboi, N., Bahr, J., Balandin, V., Beutner, B., Brandt, A., Bolzmann, A., Brinkmann, R., Brovko, O. I., Castellano, M., Castro, P., Catani, L., Chiadroni, E., Choroba, S., Cianchi, A., Costello, J. T., Cubaynes, D., Dardis, J., Decking, W., Delsim-Hashemi, H., Delserieys, A., Di Pirro, G., Dohlus, M., Dusterer, S., Eckhardt, A., Edwards, H. T., Faatz, B., Feldhaus, J., Flottmann, K., Frisch, J., Frohlich, L., Garvey, T., Gensch, U., Gerth, C., Gorler, M., Golubeva, N., Grabosch, H. J., Grecki, M., Grimm, O., Hacker, K., Hahn, U., Han, J. H., Honkavaara, K., Hott, T., Huning, M., Ivanisenko, Y., Jaeschke, E., Jalmuzna, W., Jezynski, T., Kammering, R., Katalev, V., Kavanagh, K., Kennedy, E. T., Khodyachykh, S., Klose, K., Kocharyan, V., Korfer, M., Kollewe, M., Koprek, W., Korepanov, S., Kostin, D., Krassilnikov, M., Kube, G., Kuhlmann, M., Lewis, C. L. S., Lilje, L., Limberg, T., Lipka, D., Lohl, F., Luna, H., Luong, M., Martins, M., Meyer, M., Michelato, P., Miltchev, V., Moller, W. D., Monaco, L., Muller, W. F. O., Napieralski, A., Napoly, O., Nicolosi, P., Nolle, D., Nunez, T., Oppelt, A., Pagani, C., Paparella, R., Pchalek, N., Pedregosa-Gutierrez, J., Petersen, B., Petrosyan, B., Petrosyan, G., Petrosyan, L., Pfluger, J., Plonjes, E., Poletto, L., Pozniak, K., Prat, E., *et al.* (2007). *Nat. Photon.* **1**, 336–342.

Allaria, E., Appio, R., Badano, L., Barletta, W. A., Bassanese, S., Biedron, S. G., Borga, A., Busetto, E., Castronovo, D., Cinquegrana, P., Cleva, S., Cocco, D., Cornacchia, M., Craievich, P., Cudin, I., D'Auria, G., Dal Forno, M., Danailov, M. B., De Monte, R., De Ninno, G., Delgiusto, P., Demidovich, A., Di Mitri, S., Diviacco, B., Fabris, A., Fabris, R., Fawley, W., Ferianis, M., Ferrari, E., Ferry, S., Froehlich, L., Furlan, P., Gaio, G., Gelmetti, F., Giannessi, L., Giannini, M., Gobessi, R., Ivanov, R., Karantzoulis, E., Lonza, M., Lutman, A., Mahieu, B., Milloch, M., Milton, S. V., Musardo, M., Nikolov, I., Noe, S., Parmigiani, F., Penco, G., Petronio, M., Pivetta, L., Predonzani, M., Rossi, F., Rumiz, L., Salom, A., Scafuri, C., Serpico, C., Sigalotti, P., Spampinati, S., Spezzani, C., Svandrlik, M., Svetina, C., Tazzari, S., Trovo, M., Umer, R., Vascotto, A., Veronese, M., Visintini, R., Zaccaria, M., Zangrando, D. & Zangrando, M. (2012). *Nat. Photon.* **6**, 699–704.

Alotaibi, B. M., Altuijri, R., Habib, A. F., Hala, A., Hidding, B., Khalil, S. M., McNeil, B. W. J. & Traczykowski, P. (2020). *New J. Phys.* **22**, 013037.

Anania, M. P., Brunetti, E., Wiggins, S. M., Grant, D. W., Welsh, G. H., Issac, R. C., Cipiccia, S., Shanks, R. P., Manahan, G. G., Aniculaesei, C., van der Geer, S. B., de Loos, M. J., Poole, M. W., Shepherd, B. J. A., Clarke, J. A., Gillespie, W. A., MacLeod, A. M. & Jaroszynski, D. A. (2014). *Appl. Phys. Lett.* **104**, 264102.

André, T., Andriyash, I. A., Loulergue, A., Labat, M., Roussel, E., Ghaith, A., Khojoyan, M., Thaury, C., Valléau, M., Briquez, F., Marteau, F., Tavakoli, K., N'Gotta, P., Dietrich, Y., Lambert, G., Malka, V., Benabderrahmane, C., Vétéran, J., Chapuis, L., El Ajjouri, T., Sebdaoui, M., Hubert, N., Marcouillé, O., Berteaud, P., Leclercq, N., El Ajjouri, M., Rommeluère, P., Bouvet, F., Duval, J., Kitegi, C., Blache, F., Mahieu, B., Corde, S., Gautier, J., Ta Phuoc, K., Goddet, J. P., Lestrade, A., Herbeaux, C., Évain, C., Szwaj, C., Bielawski, S., Tafzi, A., Rousseau, P., Smartsev, S., Polack, F., Dennetière, D., Bourassin-Bouchet, C., De Oliveira, C. & Couprie, M. E. (2018). *Nat. Commun.* **9**, 1334.

Balandin, V. & Golubeva, N. (2017). *Proceedings of the 8th International Particle Accelerator Conference (IPAC2017)*, 14–19 May, 2017, Copenhagen, Denmark, pp. 686–688. MOPIK069.

Borland, M. (2001). *Phys. Rev. ST Accel. Beams* **4**, 070701.

Brynes, A. D., Smorenburg, P., Akkermans, I., Allaria, E., Badano, L., Brussaard, S., Danailov, M., Demidovich, A., De Ninno, G., Gauthier, D., Gaio, G., van der Geer, S. B., Giannessi, L., de Loos, M. J., Mirian, N. S., Penco, G., Rebernik, P., Rossi, F., Setija, I., Spampinati, S., Spezzani, C., Trovò, M., Williams, P. H. & Di Mitri, S. (2018). *New J. Phys.* **20**, 073035.

Chao, A. W., Mess, K. H., Tigner, M. & Zimmermann, F. (2013). *Handbook of Accelerator Physics and Engineering.* Singapore: World scientific.

Couprie, M. E., Labat, M., Evain, C., Marteau, F., Briquez, F., Khojoyan, M., Benabderrahmane, C., Chapuis, L., Hubert, N., Bourassin-Bouchet, C., El Ajjouri, M., Bouvet, F., Dietrich, Y., Valléau, M., Sharma, G., Yang, W., Marcouillé, O., Vétéran, J., Berteaud, P., El Ajjouri, T., Cassinari, L., Thaury, C., Lambert, G., Andriyash, I., Malka, V., Davoine, X., Tordeux, M. A., Miron, C., Zerbib, D., Tavakoli, K., Marlats, J. L., Tilmont, M., Rommeluère, P., Duval, J. P., N'Guyen, M. H., Rouqier, A., Vanderbergue, M., Herbeaux, C., Sebdouai, M., Lestrade, A., Leclercq, N., Dennetière, D., Thomasset, M., Polack, F., Bielawski, S., Szwaj, C. & Loulergue, A. (2016). *Plasma Phys. Control. Fusion*, **58**, 034020.

Dattoli, G., Doria, A., Sabia, E. & Artioli, M. (2017). *Charged Beam Dynamics, Particle Accelerators and Free Electron Lasers.* Bristol, UK: IOP Publishing.

Deng, H., Decking, W. & Faatz, B. (2011). *arXiv*:1103.0112.

Emma, P., Akre, R., Arthur, J., Bionta, R., Bostedt, C., Bozek, J., Brachmann, A., Bucksbaum, P., Coffee, R., Decker, F. J., Ding, Y., Dowell, D., Edstrom, S., Fisher, A., Frisch, J., Gilevich, S., Hastings, J., Hays, G., Hering, P., Huang, Z., Iverson, R., Loos, H., Messerschmidt, M., Miahnahri, A., Moeller, S., Nuhn, H. D., Pile, G., Ratner, D., Rzepiela, J., Schultz, D., Smith, T., Stefan, P., Tompkins, H., Turner, J., Welch, J., White, W., Wu, J., Yocky, G. & Galayda, J. (2010). *Nat. Photon.* **4**, 641–647.

Esarey, E., Schroeder, C. B. & Leemans, W. P. (2009). *Rev. Mod. Phys.* **81**, 1229–1285.

Feng, C., Xiang, D., Deng, H., Huang, D., Wang, D. & Zhao, Z. (2015). *Opt. Express*, **23**, 14993–15002.

Feng, K., Yu, C., Liu, J., Wang, W., Tian, Y., Zhang, Z., Qi, R., Fang, M., Liu, J., Qin, Z., Wu, Y., Chen, Y., Ke, L., Wang, C. & Li, R. (2018). *Opt. Express*, **26**, 19067–19079.

Fuchs, M., Weingartner, R., Popp, A., Major, Z., Becker, S., Osterhoff, J., Cortrie, I., Zeitler, B., Hörlein, R., Tsakiris, G. D., Schramm, U., Rowlands-Rees, T. P., Hooker, S. M., Habs, D., Krausz, F., Karsch, S. & Grüner, F. (2009). *Nat. Phys.* **5**, 826–829.

Fukuzawa, H. & Ueda, K. (2020). *Adv. Phys. X*, **5**, 1785327.

Ghaith, A., Kitegi, C., André, T., Valléau, M., Marteau, F., Vétéran, J., Blache, F., Benabderrahmane, C., Cosson, O., Forest, F., Jivkov, P., Lancelot, J. L. & Couprie, M. E. (2018). *Nucl. Instrum. Methods Phys. Res. A*, **909**, 290–293.

Ghaith, A., Oumbarek, D., Kitégi, C., Valléau, M., Marteau, F. & Couprie, M.-E. (2019). *Instruments* **3**, 27.

Gover, A. (2005). *Phys. Rev. ST Accel. Beams* **8**, 030701.

Hemsing, E. (2018). *Phys. Rev. Accel. Beams*, **21**, 050702.

Huang, Z. R., Ding, Y. T. & Schroeder, C. B. (2012). *Phys. Rev. Lett.* **109**, 204801.

Ishikawa, T., Aoyagi, H., Asaka, T., Asano, Y., Azumi, N., Bizen, T., Ego, H., Fukami, K., Fukui, T., Furukawa, Y., Goto, S., Hanaki, H., Hara, T., Hasegawa, T., Hatsui, T., Higashiya, A., Hirono, T., Hosoda, N., Ishii, M., Inagaki, T., Inubushi, Y., Itoga, T., Joti, Y., Kago, M., Kameshima, T., Kimura, H., Kirihara, Y., Kiyomichi, A., Kobayashi, T., Kondo, C., Kudo, T., Maesaka, H., Maréchal, X. M., Masuda, T., Matsubara, S., Matsumoto, T., Matsushita, T., Matsui, S., Nagasono, M., Nariyama, N., Ohashi, H., Ohata, T., Ohshima, T., Ono, S., Otake, Y., Saji, C., Sakurai, T., Sato, T., Sawada, K., Seike, T., Shirasawa, K., Sugimoto, T., Suzuki, S., Takahashi, S., Takebe, H., Takeshita, K., Tamasaku, K., Tanaka, H., Tanaka, R., Tanaka, T., Togashi, T., Togawa, K., Tokuhisa, A., Tomizawa, H., Tono, K., Wu, S., Yabashi, M., Yamaga, M., Yamashita, A., Yanagida, K., Zhang, C., Shintake, T., Kitamura, H. & Kumagai, N. (2012). *Nat. Photon.* **6**, 540–544.

Jia, Q. K. & Li, H. T. (2017). *Phys. Rev. Accel. Beams*, **20**, 020707.

Khan, D. & Raubenheimer, T. (2014). *Proceedings of the 36th International Free Electron Laser Conference (FEL2014)* 25–29 August, 2014, Basel, Switzerland, pp. 755–762. THP027.

Kim, K.-J., Huang, Z. & Lindberg, R. (2017). *Synchrotron Radiation and Free-Electron Lasers: Principles of Coherent X-ray Generation.* Cambridge University Press.

Labat, M., Bielawski, S., Loulergue, A., Corde, S., Couprie, M. E. & Roussel, E. (2020). *New J. Phys.* **22**, 013051.

Leemans, W. P., Gonsalves, A. J., Mao, H. S., Nakamura, K., Benedetti, C., Schroeder, C. B., Tóth, C., Daniels, J., Mittelberger, D. E., Bulanov, S. S., Vay, J. L., Geddes, C. G. & Esarey, E. (2014). *Phys. Rev. Lett.* **113**, 245002.

Lindstrøm, C. A. & Adli, E. (2016). *Phys. Rev. Accel. Beams*, **19**, 071002.

Liu, T., Feng, C., Xiang, D., Liu, J. & Wang, D. (2019). *J. Synchrotron Rad.* **26**, 311–319.

Liu, W. H., Jiao, Y. & Wang, S. (2020). *Nucl. Instrum. Methods Phys. Res. A*, **983**, 164605.

Loulergue, A., Labat, M., Evain, C., Benabderrahmane, C., Malka, V. & Couprie, M. E. (2015). *New J. Phys.* **17**, 023028.

Madey, J. M. J. (1971). *J. Appl. Phys.* **42**, 1906–1913.

Maier, A. R., Delbos, N. M., Eichner, T., Hübner, L., Jalas, S., Jeppe, L., Jolly, S. W., Kirchen, M., Leroux, V., Messner, P., Schnepp, M., Trunk, M., Walker, P. A., Werle, C. & Winkler, P. (2020). *Phys. Rev. X*, **10**, 031039.

Pollock, B. B., Clayton, C. E., Ralph, J. E., Albert, F., Davidson, A., Divol, L., Filip, C., Glenzer, S. H., Herpoldt, K., Lu, W., Marsh, K. A., Meinecke, J., Mori, W. B., Pak, A., Rensink, T. C., Ross, J. S.,

Shaw, J., Tynan, G. R., Joshi, C. & Froula, D. H. (2011). *Phys. Rev. Lett.* **107**, 045001.
Qin, W. L., Zeng, L., Huang, S. L., Zhao, G., Ding, Y. T., Huang, Z. R., Hu, R. H., Lu, H. Y., Yan, X. Q. & Liu, K. X. (2019). *Nucl. Instrum. Methods Phys. Res. A*, **925**, 193–198.
Reiche, S. (1999). *Nucl. Instrum. Methods Phys. Res. A*, **429**, 243–248.
Rossbach, J., Schneider, J. R. & Wurth, W. (2019). *Phys. Rep.* **808**, 1–74.
Schlenvoigt, H. P., Haupt, K., Debus, A., Budde, F., Jäckel, O., Pfotenhauer, S., Schwoerer, H., Rohwer, E., Gallacher, J. G., Brunetti, E., Shanks, R. P., Wiggins, S. M. & Jaroszynski, D. A. (2008). *Nat. Phys.* **4**, 130–133.
Seddon, E. A., Clarke, J. A., Dunning, D. J., Masciovecchio, C., Milne, C. J., Parmigiani, F., Rugg, D., Spence, J. C. H., Thompson, N. R., Ueda, K., Vinko, S. M., Wark, J. S. & Wurth, W. (2017). *Rep. Prog. Phys.* **80**, 115901.
Tajima, T. & Dawson, J. M. (1979). *Phys. Rev. Lett.* **43**, 267–270.
Thaury, C., Guillaume, E., Döpp, A., Lehe, R., Lifschitz, A., Ta Phuoc, K., Gautier, J., Goddet, J. P., Tafzi, A., Flacco, A., Tissandier, F., Sebban, S., Rousse, A. & Malka, V. (2015). *Nat. Commun.* **6**, 6860.
Thaury, C., Guillaume, E., Lifschitz, A., Ta Phuoc, K., Hansson, M., Grittani, G., Gautier, J., Goddet, J. P., Tafzi, A., Lundh, O. & Malka, V. (2015). *Sci. Rep.* **5**, 16310.
Wang, X. F., Feng, C., Tsai, C. Y., Zeng, L. & Zhao, Z. T. (2019). *Phys. Rev. Accel. Beams*, **22**, 070701.
Xiang, D. & Wan, W. (2010). *Phys. Rev. Lett.* **104**, 084803.
Yu, L. H. (1991). *Phys. Rev. A*, **44**, 5178–5193.
Zhang, T., Feng, C., Deng, H., Wang, D., Dai, Z. & Zhao, Z. (2014). *Opt. Express*, **22**, 13880–13888.